Briefs

Geometric Analysis of Solar Cells With Partial Rear Contacts: Comparison to 3-D Simulations

Andres Cuevas, *Senior Member, IEEE*, and Jan H. Petermann

***Abstract*—A geometric approach to analyze solar cells with local rear contacts has been proposed in a recent paper. This brief presents an extension to it based on numerical iteration that permits us to determine *I–V* characteristic curves and conversion efficiencies. A good agreement with 3-D Sentaurus Device simulations is observed.**

***Index Terms*—Modeling, partial rear contact solar cells.**

I. Introduction

In a recent paper [1], one of us proposed to study silicon solar cells with localized rear contacts using a geometric approach which is based on subdividing the device into two main regions: one close to the contact and the other peripheral to it. The approach was used to derive the open-circuit voltage $V_{\rm oc}$ and the series resistance R_s and found to be in good agreement with a prior analytical model by Fischer [2].

In [1], it was mentioned that an iterative procedure would be needed in order to study cases where the minority carrier concentration is not uniform at the front surface of the solar cell. A further enhancement to the geometric approach is presented here, using numerical iteration to better account for recombination in the peripheral region of the device. As a bonus, the iterative method makes it possible to determine the full I–V curve of the solar cell and its conversion efficiency. To assess its validity, we compare the iterative version of the geometric model with the 3-D simulation program Sentaurus Device [3], finding both in good agreement.

II. Summary of the Geometric Model

The elementary solar cell can be divided into two regions: one directly above and near the contact and a second region peripheral to the first. For details, see [1].

A. Near-Contact Region

Except for those that recombine at the front surface or in the bulk, minority carriers converge toward the contact through a shrinking cross-sectional area $A(x)$. An appropriate function to describe it is

$$A(x) = \pi a^2 + \pi^2 a(W - x) + 2\pi(W - x)^2 \tag{1}$$

where x is the vertical distance from the front junction, a is the radius of the contact, and W is the wafer thickness. We can determine the minority carrier concentration at the front pn-junction n_f by the integration of the diffusion current

$$n_f = n_b + \frac{A_0}{qD_n}\int_W^0 \frac{J_n}{A(x)}dx. \tag{2}$$

In (2), J_n and D_n are the electron current density and diffusivity, respectively, and A_0 is the aperture area of the unit cell, with $A_0 = P^2$ for a square arrangement of contacts separated a distance P. The carrier concentration at the back contact n_b is given by

$$n_b = \frac{J_n(W)}{q(f_c/f_{\rm NC})S_{\rm cont}} \tag{3}$$

where f_c is the fraction of the rear surface from which current is extracted, $f_{\rm NC} = \pi y_{\rm min}^2/A_0$ is the fractional area of the near-contact region, $J_n(W)$ is the electron current reaching the contact, and $S_{\rm cont}$ is the surface recombination velocity of the contact. Additional equations, which may be found in [4], relate the electron, hole, and total currents to the generation and recombination occurring in the volume of the material. Surface boundary conditions are expressed in terms of a recombination current prefactor J_o.

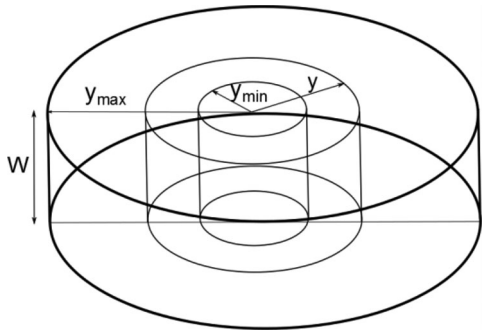

Fig. 1. Schematic diagram of the geometry used to analyze the lateral region.

B. Peripheral Region

We represent the unit solar cell by means of a cylindrical geometry as depicted in Fig. 1, with an outer radius $y_{\rm max} = (A_0/\pi)^{1/2}$ and an inner cylinder of radius $y_{\rm min} = a + W\pi/4$ that defines the boundary with the near-contact region [1]. Considering now a cylindrical element in the lateral direction y, it will contribute to the majority carrier current an amount that results from the local balance between generation and recombination

$$I_p(y) = I_p(y + dy) + (J_{\rm ph} - J_{\rm rec})2\pi y dy \tag{4}$$

where $J_{\rm rec}$ may include bulk and surface (front and rear) recombination. To calculate it, we have assumed that the minority carrier concentration within an elementary volume is approximately constant in the vertical direction and equal to its value at the front $n_f(y)$. Such an assumption is appropriate in many cases of practical interest when the minority carrier diffusion length is greater than the wafer thickness and when the rear surface is well passivated. It can be inadequate, however, if bulk or rear surface recombination is severe.

The majority carrier (hole) current is driven by a gradient of the electrostatic potential ϕ

$$I_p(y) = -\sigma_p A(y)\frac{d\phi}{dy} \tag{5}$$

Manuscript received July 24, 2012; revised September 11, 2012; accepted September 20, 2012. Date of publication October 15, 2012; date of current version December 19, 2012.

A. Cuevas is with the Australian National University, Canberra, A.C.T 0200, Australia (e-mail: andres.cuevas@anu.edu.au).

J. H. Petermann is with the Institute for Solar Energy Research Hameln, 31860 Emmerthal, Germany (e-mail: j.petermann@isfh.de).

Color versions of one or more of the figures in this paper are available online at http://ieeexplore.ieee.org.

Digital Object Identifier 10.1109/JPHOTOV.2012.2221084

where the cross-sectional area is $A(y) = 2\pi yW$, and σ_p is the hole conductivity (see Fig. 1). The electrostatic potential difference as a function of the lateral position can be obtained by the integration of (5). The minority carrier concentration in the lateral direction y can then be determined from

$$n_f(y)(p_o + n_f(y)) = n_i^2 \exp\left(\frac{\phi(y)}{kT/q}\right) \tag{6}$$

where $p_0 \approx N_A$ is the majority carrier concentration. An iterative procedure starts by giving an initial value to the minority carrier concentration at the extreme position of the unit cell, $n_f(y_{\max})$. The net current $I_p(y_{\min})$ injected by the peripheral region into the near-contact region is then calculated. The minority carrier concentration $n_f(y_{\min})$ at the inner position of the unit cell is then used in conjunction with (2) to determine the carrier profile in the near-contact region, that is, in the x-direction. An open-circuit solution is found by iterating the value of $n_f(y_{\max})$ until a global balance between the total generation and recombination in the unit cell is established. Complete $I-V$ characteristics can be determined by varying $n_f(y_{\max})$ and iterating the carrier density profile until it is consistent with the corresponding output current and the boundary conditions. The iterative process can be implemented with relative ease using, for example, Microsoft Excel and its Visual Basic capabilities.

III. Comparison to 3-D Simulations

A. Simulation Parameters

To analyze a partial rear contact cell structure in Sentaurus Device, we have used square contacts arranged in a square pattern with the same area as circular contacts of radius $a = 100\ \mu$m, together with the silicon parameters of [5]. A front n^+ diffused region having a Gaussian dopant profile with a surface concentration of 10^{20} cm^{-3} and a junction depth of 0.75 μm, together with a front surface recombination velocity of $1.5 \cdot 10^4$ cm$\cdot$s^{-1}, produces a recombination that can be characterized in the geometric model by a recombination current prefactor of $J_{0f} = 100$ fA$\cdot$cm^{-2}. We verified this J_{0f} by simulating a sample akin to those used for the experimental measurement of J_{0f} by photoconductance decay, that is, with a base dopant concentration of 10^{13} cm^{-3}, the aforementioned dopant profile on one side, and negligible bulk recombination.

The diffused region presents a sheet resistance of 35 Ω, which also contributes slightly to the lateral voltage drop due to the flow of electrons through it. In the geometric model, we have added an extra term to the conductivity in (5) to account for such lateral voltage drop, noting that the electron current at a given lateral position y is equal to the hole current at that position. In this example, we have only included intrinsic bulk recombination and set to zero the recombination at the passivated areas of the rear surface. The temperature is 300 K, and the photogeneration corresponds to that produced by the AM1.5G spectrum, together with front surface texturing and a good back surface mirror.

B. Simulation Results

Figs. 2–5 show the results of both Sentaurus Device simulations and the iterative geometric model for a p-type silicon wafer with $N_A = 10^{16}$ cm^{-3} and $W = 180\ \mu$m. The circular contacts have a radius of 100 μm and either a very high $S_{\rm cont} = 10^6$ cm$\cdot$s^{-1}, a moderate $S_{\rm cont} = 10^4$ cm$\cdot$s^{-1}, or a very low $S_{\rm cont} = 332$ cm$\cdot$s^{-1} surface recombination velocity. The latter is equivalent to a recombination current prefactor of $J_{0\rm cont} = 500$ fA$\cdot$cm^{-2}, representative of optimized p^+ doped regions that are formed by alloying aluminum into silicon [6].

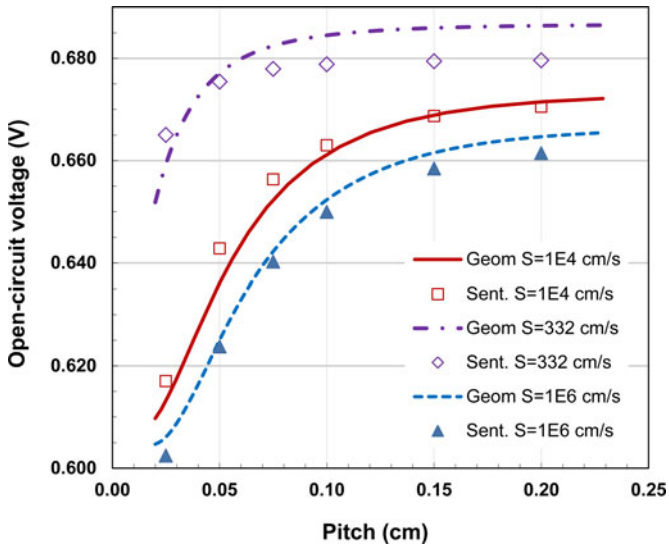

Fig. 2. Open-circuit voltage as a function of the pitch for $N_A = 10^{16}$ cm^{-3}, $a = 100\ \mu$m, $W = 180\ \mu$m, and $J_{0f} = 10^{-13}$ A$\cdot$cm^{-2}. Geometric model for $S_{\rm cont} = 332$ cm$\cdot$s^{-1} (dot-dashed line), $S_{\rm cont} = 10^4$ cm$\cdot$s^{-1} (continuous line), and $S_{\rm cont} = 10^6$ cm$\cdot$s^{-1} (dashed line) compared with Sentaurus simulations (open diamonds, open squares, and filled triangles, respectively).

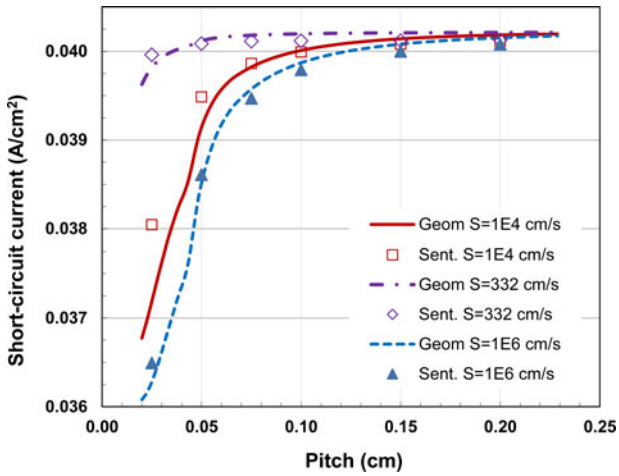

Fig. 3. Short-circuit current density as a function of the pitch for $N_A = 10^{16}$ cm^3, $a = 100\ \mu$m, $W = 180\ \mu$m, and $J_{0f} = 10^{-13}$ A$\cdot$cm^{-2}. Geometric model for $S_{\rm cont} = 332$ cm$\cdot$s^{-1} (dot-dashed line), $S_{\rm cont} = 10^4$ cm$\cdot$s^{-1} (continuous line), and $S_{\rm cont} = 10^6$ cm$\cdot$s^{-1} (dashed line) compared with Sentaurus simulations (open diamonds, open squares, and filled triangles, respectively).

The open-circuit voltage $V_{\rm oc}$ as a function of the pitch, or separation between the contacts, is shown in Fig. 2. As expected, $V_{\rm oc}$ increases with the pitch and with the degree of passivation of the contact. The values which are calculated with the geometric model are within 6 mV of the corresponding Sentaurus simulations, which is the largest discrepancy occurring for the case of a well-passivated contact.

The short-circuit current density $J_{\rm sc}$, which is shown in Fig. 3, also increases with the same parameters as $V_{\rm oc}$. The geometric model underestimates $J_{\rm sc}$ for low-pitch values. This could be due to small differences in the way that the boundary condition (3) is applied or to the different shape of the contacts implemented in both models.

The agreement in terms of the fill factor, which is shown in Fig. 4, is very good. The main result is that, as expected, the *FF* degrades severely for large pitch values.

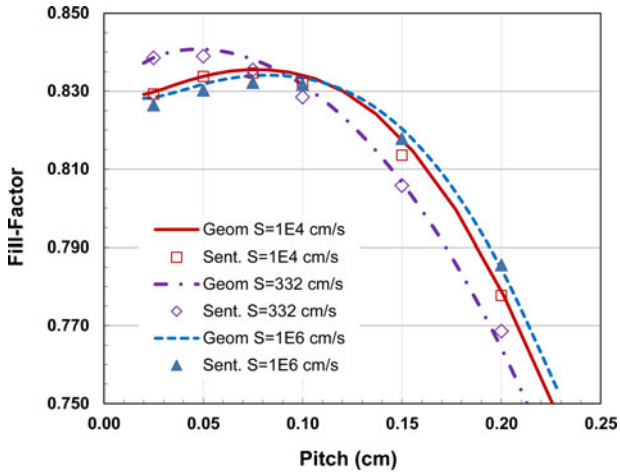

Fig. 4. Fill factor as a function of the pitch for $N_A = 10^{16}$ cm^{-3}, $a = 100\,\mu$m, $W = 180\,\mu$m, and $J_{0f} = 10^{-13}$ A $\cdot$ cm^{-2}. Geometric model for $S_{\rm cont} = 332$ cm $\cdot$ s^{-1} (dot-dashed line), $S_{\rm cont} = 10^4$ cm $\cdot$ s^{-1} (continuous line), and $S_{\rm cont} = 10^6$ cm $\cdot$ s^{-1} (dashed line), compared with Sentaurus simulations (open diamonds, open squares, and filled triangles, respectively).

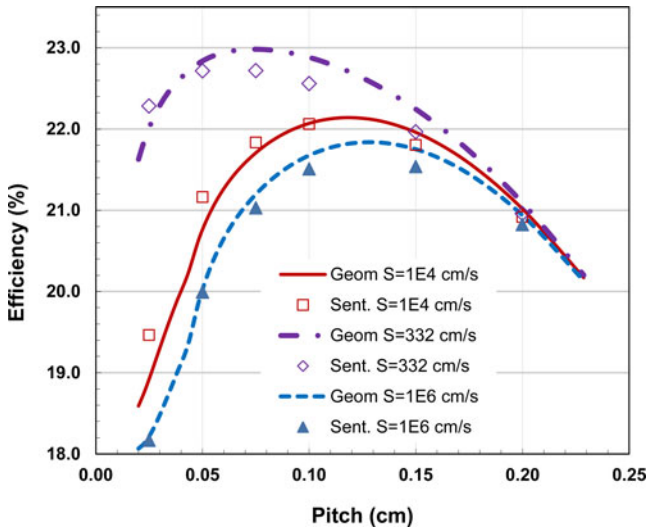

Fig. 5. Conversion efficiency as a function of the pitch for $N_A = 10^{16}$ cm^{-3}, $a = 100\,\mu$m, $W = 180\,\mu$m, and $J_{0f} = 10^{-13}$ A $\cdot$ cm^{-2}. Geometric model for $S_{\rm cont} = 332$ cm $\cdot$ s^{-1} (dot-dashed line), $S_{\rm cont} = 10^4$ cm $\cdot$ s^{-1} (continuous line), and $S_{\rm cont} = 10^6$ cm $\cdot$ s^{-1} (dashed line), compared with Sentaurus simulations (open diamonds, open squares, and filled triangles, respectively).

The combination of the aforementioned three parameters results in a conversion efficiency that, as shown in Fig. 5, presents a maximum just before the improvements in $V_{\rm oc}$, and $J_{\rm sc}$ are negated by the degradation in FF. The agreement between the geometric approach and Sentaurus is reasonably good for the three cases of contact recombination velocity. Both simulations indicate that the optimum pitch is smaller as the passivation of the contact is improved. For nonpassivated contacts, it should be approximately 0.125 cm, whereas for well-passivated contacts, it should be approximately 0.075 cm. The geometric model predicts the trends reasonably well, with a discrepancy with respect to Sentaurus of less than 0.3 absolute efficiency points in the vicinity of the optimum pitch.

IV. Conclusion

Although not exhaustive, the comparison presented here indicates a good agreement between 3-D simulations and the geometric approach proposed in [1]. The latter, in its iterative implementation, may be regarded as a numerical analysis of the device, but a simple one. We have used 100 elements in the lateral direction and 200 in the vertical one, that is, a total of 300, with no attempt to optimize their number. For the dopant density in these calculations, low injection conditions prevail. Further testing and comparison are needed to fully assess the range of applicability of the geometric-iterative approach. It is likely that the simplifications underlying it will cease to apply if recombination in the bulk or at the dielectric-coated regions of the back surface becomes significant, in which detailed numerical simulations remain necessary.

Acknowledgment

The authors would like to thank F. Haase and P. Altermatt from ISFH for helpful discussions and T. Ohrdes from ISFH for making the graphical user interface for Sentaurus Device available.

References

[1] A. Cuevas, "Geometrical analysis of solar-cells with partial rear contacts," *IEEE J. Photovoltaics*, vol. 2, no. 4, pp. 485–493, Oct. 2012.
[2] B. Fischer, "Loss analysis of crystalline silicon solar cells using photoconductance and quantum efficiency measurements," Ph.D. dissertation, Univ. Konstanz, Konstanz, Germany, 2003.
[3] *Sentaurus Process User Guide, Version E-2010.12*, Synopsys, Inc., Mountain View, CA, 2010.
[4] A. Cuevas, "Modelling silicon characterisation," *Energy Procedia*, vol. 8, pp. 94–99, 2011.
[5] P. P. Altermatt, "Models for numerical device simulations of crystalline silicon solar cells—A review," *J. Comput. Electron.*, vol. 10, pp. 314–330, 2011.
[6] R. Woehl, P. Gundel, J. Krause, K. Rühle, F. D. Heinz, M. Rauer, C. Schmiga, M. C. Schubert, W. Warta, and D. Biro, "Evaluating the aluminum-alloyed p^+-layer of silicon solar cells by emitter saturation current density and optical microspectroscopy measurements," *IEEE Trans. Electron Devices*, vol. 58, no. 2, pp. 441–447, Feb. 2011.